Textures and Microstructures, Vol. 30, pp. 81–95
Reprints available directly from the publisher
Photocopying permitted by license only

TEXTURE AND STRUCTURE EVOLUTION DURING INDIRECT EXTRUSION OF AN AlSiMgMn ALUMINIUM ALLOY

HANS ERIK VATNE [a,*], KETILL PEDERSEN [b], OTTO LOHNE [b] and GAUTE JENSSEN [c]

[a] *Formerly at SINTEF, now with Hydro Aluminium, R&D Materials Technology, N-6601 Sunndalsøra, Norway;* [b] *SINTEF Materials Technology, Alfred Getzv. 2B, N-7034 Trondheim, Norway;* [c] *Raufoss Technology, Box 77, N-2831 Raufoss, Norway*

(Received 16 May 1997)

Texture evolution during indirect extrusion of cylindrical profiles of an AlSiMgMn aluminium alloy was investigated in the present work. The effect of extrusion temperature on texture development, through-thickness texture variations and texture variations along the length of the extruded profiles were investigated. In all cases a combined ⟨100⟩ and ⟨111⟩ fibre texture developed. Generally, the ⟨111⟩ fibre was sharper than the ⟨100⟩ fibre. The texture evolution was rather similar along the length of the profile, while the variations through the thickness were considerable. In a region midways between the centre and the surface of the profiles, the ⟨100⟩ fibre was weakened, and in the surface regions the two fibres were significantly rotated. The texture measurements showed a strong dependence on extrusion temperature, in the sense that the higher the temperature, the sharper the ⟨100⟩ fibre texture. The influence of texture variations on formability were also investigated.

Keywords: Indirect extrusion; Aluminium alloy; Deformation texture; Subgrain size; Misorientation; Inhomogeneity

1. INTRODUCTION

Extrusion is an important industrial process. Usually, extrusion is performed by a direct method, i.e. the extrusion billet is pressed through a stationary die. An alternative is indirect extrusion where the billet is

* Corresponding author. Tel.: (+47) 7169 3608. Fax: (+47) 7169 3602.

stationary and the die is pressed towards the billet. The latter has the advantage of a lower required ram force due to a slightly different flow pattern. The different flow pattern would also be expected to give a different texture evolution. While texture evolution during direct extrusion has been reported in the literature, results from indirect extrusion are not well known. The texture aspect has been investigated in detail in the present work. In this investigation the effect of a variation in extrusion temperature has been focused, and also the texture variations through the thickness and along a profile have been characterized. Further, the influence of texture variations on formability has been studied. The latter is important since extruded profiles are often subjected to subsequent forming operations like forging and bending.

2. EXPERIMENTAL

An AA6082 (Al–1wt%Si–0.6wt%Mg–0.5wt%Mn) was investigated. Cylindrical profiles of diameter 36 mm were extruded from billets of diameter 203 mm and length 750 mm, i.e. the area reduction ratio was $A_0/A = 32$ ($\varepsilon = \ln[A_0/A] = 3.5$) and the profile length was of the order 20 m. Prior to extrusion the billets were homogenized for 12 h at 520°C. Extrusion was undertaken at a range of deformation temperatures, for details see Table I. All profiles were cooled in air.

Textures were investigated by means of a Siemens D5000 X-ray diffractometer. The substructure (subgrain size and misorientations between subgrains) of the deformation texture components were

TABLE I Pre-heating and deformation conditions for indirect extrusion of the AA6082 cylindrical profiles (diameter 36 mm)

	Sample				
	IE1	IE2	IE3	IE4	IE5
Homogenization Temp./Time	520°C/12 h	520°C/12 h	520°C/12 h	520°C/12 h	520°C/12 h
Container Temperature	430°C	430°C	430°C	430°C	430°C
Billet Temp. front	502°C	501°C	437°C	532°C	542°C
Billet Temp. middle	507°C	502°C	445°C	546°C	551°C
Billet Temp. back	492°C	496°C	447°C	540°C	538°C
Profile Temp. front	502°C	500°C	480°C	544°C	548°C
Profile Temp. middle	520°C	543°C	484°C	542°C	538°C
Profile Temp. back	500°C	515°C	470°C	527°C	506°C
Extrusion speed	7.2 m/min	14.4 m/min	12 m/min	12 m/min	8 m/min

investigated by means of the SINTEF EBSP system attached to a Jeol 8400 SEM (Scanning Electron Microscope). In order to investigate the influence of texture on formability during subsequent forming operations, tension tests at room temperature and at elevated temperatures were performed by means of a Gleeble 3500 multi-purpose testing machine.

3. EXPERIMENTAL RESULTS

Texture Evolution

Examples of the extrusion textures are given in Fig. 1 for sample IE1. The figure shows that strong ⟨111⟩ and ⟨100⟩ fibres developed in all cases, the exception being the outer periphery where the fibres were significantly rotated. In the most extreme cases the surface textures were so strongly rotated that they approached a $\{110\}_{RD}\langle 335\rangle_{AD}$, i.e. a component with a ⟨110⟩ axis in the radial direction and a ⟨335⟩ axis in the axial direction (not so far from the $\{011\}\langle 211\rangle$ Bs deformation texture obtained in rolling of FCC metals). For the IE1 profile the textures were measured in several positions along the profile and at various distances from the surface of the profiles. In order to have a better overview of the large number of texture data, these are graphically presented in Fig. 2. In Fig. 2 the measured intensities of the ⟨100⟩ fibres, the ⟨111⟩ fibres and the ratios between them are plotted for the IE1 sample. The following observations can be made from the figure: (i) the ⟨111⟩ fibre is in all cases stronger than the ⟨100⟩ fibre, i.e. the intensity ratio ⟨100⟩/⟨111⟩ is less than one. (ii) The texture is rather similar along the length of the profile. (iii) An interesting drop in the strength of the ⟨100⟩ fibre is seen in the region $S=0.25$–0.6. The parameter S is defined as $S=0$ in the centre and $S=1$ at the surface of the profiles, i.e. the region with the weak ⟨100⟩ fibre is located midways between the centre and the surface. This texture difference has the following effect on the average Taylor factors of specimen IE1: $M_{S=0}=3.17$ for the $S=0$ sample (centre) and $M_{S=0.5}=3.34$ for the $S=0.5$ sample. The Taylor factors were calculated by means of the software "MTM Taylor" (Van Houtte, 1994) under the assumption of full constraints and octahedral slip systems (⟨110⟩{111}). This difference in Taylor factor indicates variations in formability through the thickness of the profiles.

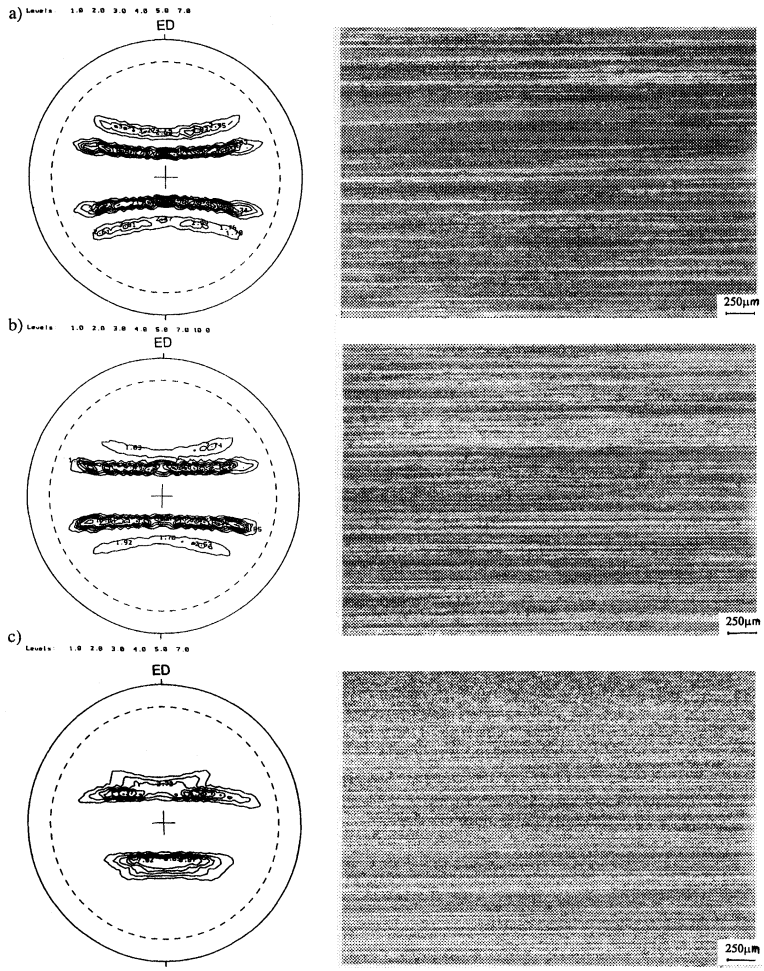

FIGURE 1 Texture ({111} pole figures) and microstructure of indirectly extruded cylindrical profiles, sample IE1, taken from the middle of the profile length at various radial (through-thickness) positions: (a) $S = 0$ (centre), (b) $S = 0.5$ and (c) $S = 1$ (surface).

Effect of Extrusion Temperature

The influence of extrusion temperature on the texture evolution was investigated in detail, with the results given in Fig. 3. The data are plotted in the same way as in Fig. 2, i.e. the intensities of the fibres are given. Notice that all samples are taken at the same position along the

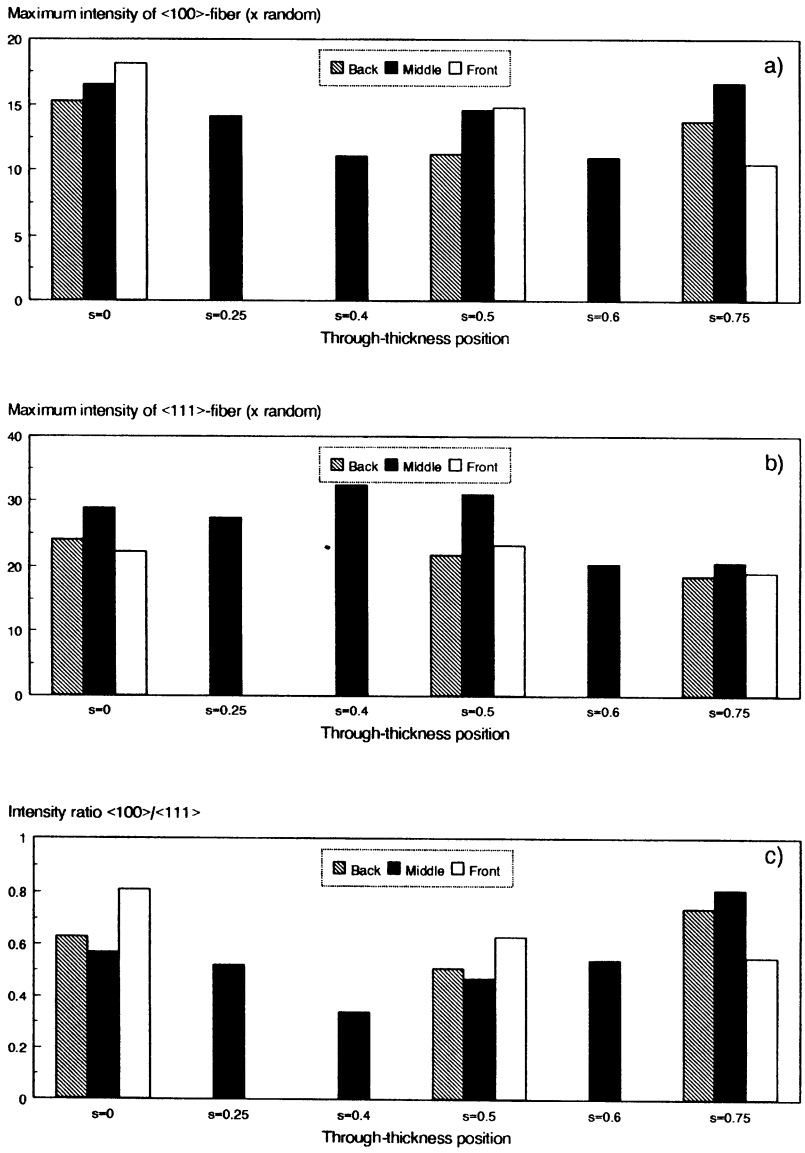

FIGURE 2 Summary of texture measurement for indirectly extruded cylindrical profiles of specimen IE1 at various through-thickness variations ($S=0$ in the centre and $S=1$ at the surface) and various positions along the profile length (front, middle, back): (a) intensity of $\langle 100 \rangle$ fibre, (b) intensity of $\langle 111 \rangle$ fibre and (c) intensity ratio $\langle 100 \rangle / \langle 111 \rangle$.

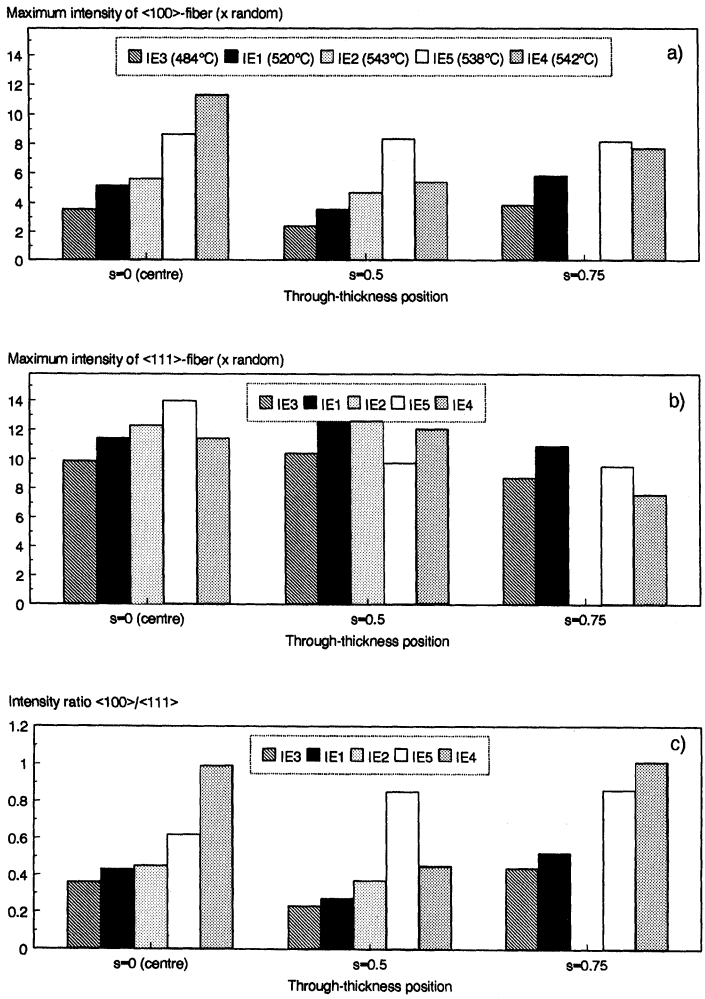

FIGURE 3 Effect of extrusion temperature on texture of indirectly extruded cylindrical profiles: (a) intensity of ⟨100⟩ fibre, (b) intensity of ⟨111⟩ fibre and (c) intensity ratio ⟨100⟩/⟨111⟩.

length of the profiles (middle), but at various radial (through-thickness) positions. The figure displays the following characteristics: (i) The profile deformed at the lowest temperature shows a very weak ⟨100⟩ fibre texture. (ii) The strength of the ⟨100⟩ fibre is strongly dependent on the extrusion temperature; the higher the temperature, the stronger the

⟨100⟩ fibre. (iii) The strength of the ⟨111⟩ fibre texture appears to be rather independent of the deformation temperature. (iv) A drop in the strength of the ⟨100⟩ fibre is seen in the region midways between the centre and the surface of the profiles.

Substructure Characterization

The substructure of the two texture fibres was characterized. This aspect was investigated for the following reasons: (i) to obtain an impression of the substructure strengthening in the two texture fibres and (ii) to enable an understanding of microstructural evolution during subsequent heat treatment (recovery and recrystallization). Two parameters were investigated; the subgrain size and the misorientation between the subgrains. The subgrain size distributions are given in Fig. 4, while the distributions of misorientations are given in Fig. 5 (sample IE1). The average subgrain size in the ⟨100⟩ component was 7.2 μm, while it was only 5.0 μm in the ⟨111⟩ fibre. Further, there is an interesting long tail of really large subgrains in the ⟨100⟩ subgrain size distribution. These large subgrains will be very potent nucleation sites for recrystallized grains during subsequent annealing. Also the average misorientation between the subgrains was significantly larger in the ⟨100⟩ component. It is obvious that the recovery reactions are extensive during the extrusion process at such a high deformation temperature and during the slow cooling after extrusion. Thus, the results indicate a much higher recovery rate in the ⟨100⟩ component than in ⟨111⟩.

The substructure data can also be used to calculate the amount of stored energy in the material. In a deformation structure consisting of a well developed subgrain structure the stored energy in a texture component will be given by

$$P_D = \alpha \frac{\gamma_{SB}}{\delta}, \tag{1}$$

where α is a geometrical constant of the order 3 for equiaxed subgrains, γ_{SB} is the subgrain boundary energy and δ is the subgrain size in the component. The subgrain boundary energy can be estimated by the Read–Schockley relation (Read, 1953):

$$\gamma_{SB} = \frac{Gb\theta}{4\pi(1-\nu)} \ln\left(\frac{e\theta_c}{\theta}\right), \tag{2}$$

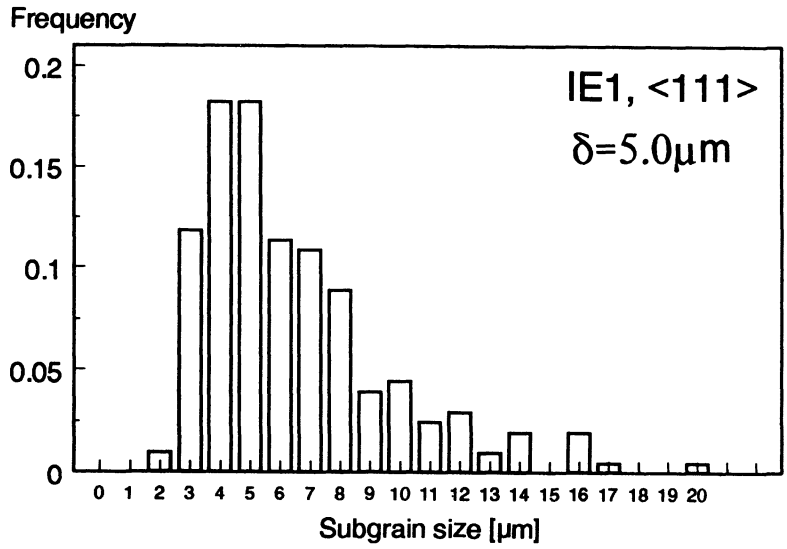

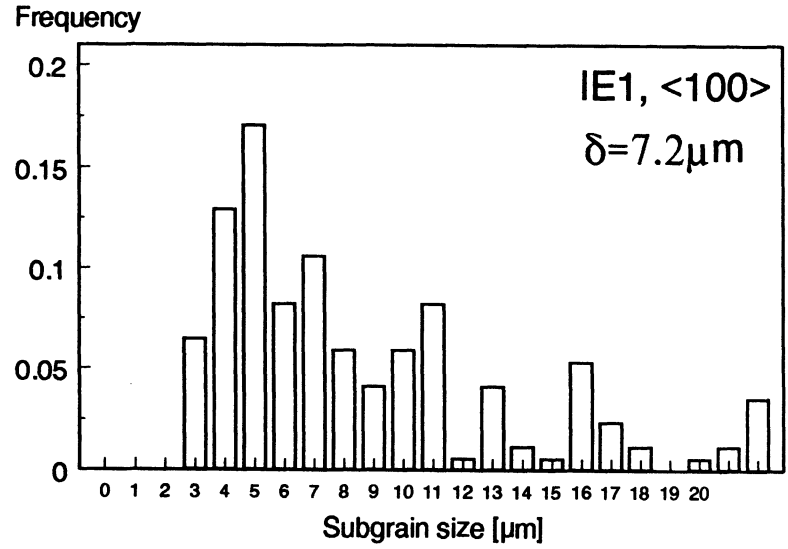

FIGURE 4 Subgrain size (δ) distributions of the two fibre texture components in material IE1, taken from the middle of the profile length near the centre ($S = 0$).

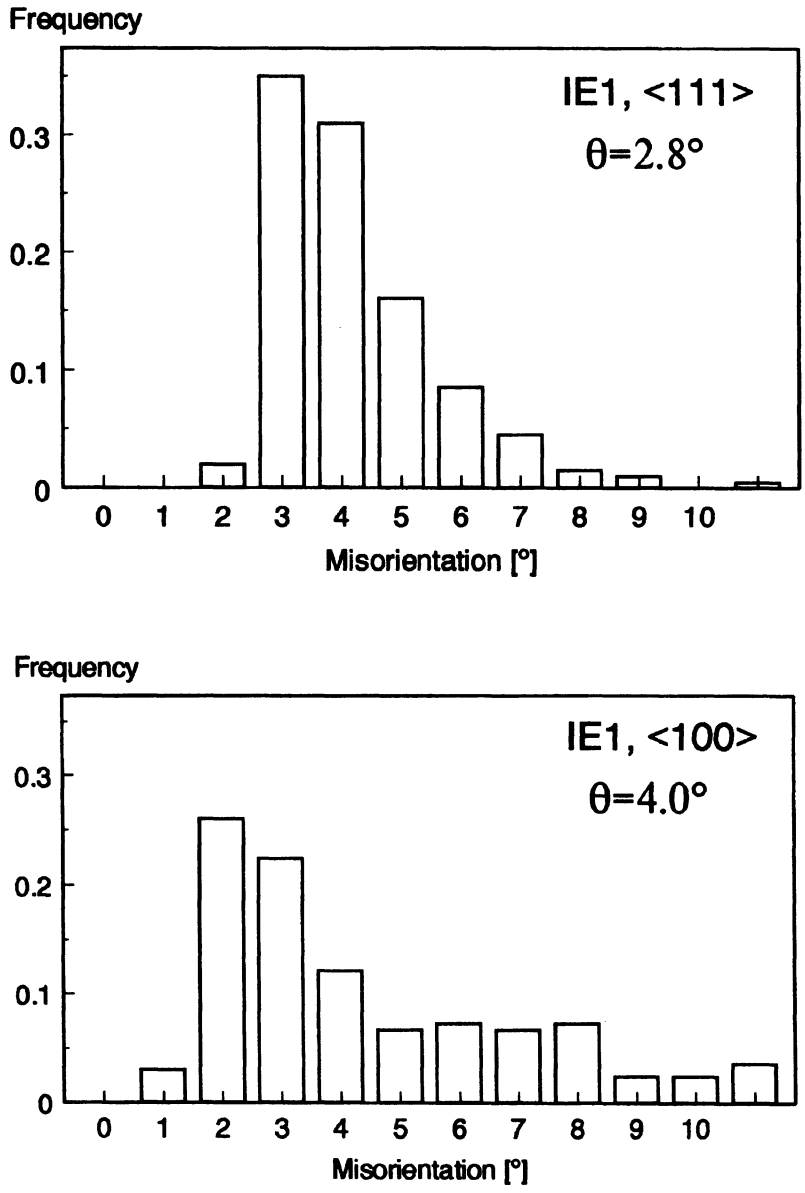

FIGURE 5 Misorientation (θ) distributions of the two fibre texture components in material IE1, taken from the middle of the profile length near the centre ($S=0$).

where θ is the misorientation between the subgrains, $G \sim 2.65 \times 10^{10}\,\mathrm{N/m^2}$ is the shear modulus, $b = 2.86 \times 10^{-10}\,\mathrm{m}$ is the Burgers vector, $\nu \sim 0.33$ is Poisson's number and $\theta_c = 15°$ is the critical value for characterising a boundary as a high angle boundary. The Read–Shockley relation should be a good approximation in the nearly equiaxed subgrain structure that is obtained during hot extrusion. By measuring the subgrain size and the misorientation between the subgrains, good estimates of the amount of stored energy in a texture component can be found by the use of Eqs. (1) and (2). It is seen from Eq. (2) that a texture component with a high amount of stored energy will be characterized by a small subgrain size and/or a high misorientation. The calculations are shown in Table II. The data in the table are based on measurements of more than 200 subgrains in each texture component. The results show that the stored energy in the ⟨100⟩ component is lower than in ⟨111⟩. The reason for this is the large subgrain size that is most likely achieved through a higher recovery rate in the ⟨100⟩ component. The higher recovery rate also leads to a higher misorientation, but still the energy is lower. Both the low stored energy and the large subgrain size indicate that subgrains of the ⟨100⟩ orientation will be potent nucleation sites for recrystallization during subsequent annealing.

Formability

In order to investigate the effect of texture on formability, tension testing was undertaken. Due to the large through-thickness texture

TABLE II Results from the EBSP characterization of the extruded material (IE1). The sample is taken from the middle of the profile length and close to the centre, δ is the average subgrain size, θ is the misorientation between subgrains, P_D is the stored energy, W_r is the average width (along the radial direction) of the texture components and f_r is the fraction of each component

	Texture component	
	⟨100⟩	⟨111⟩
δ [μm]	7.2	5.0
θ [°]	4.0	2.8
P_D [J/m^2]	6.10×10^4	7.08×10^4
W_r [μm]	14.5	17.6
f_r [%]	36.9	61.8

TABLE III Effect of texture on formability: The texture is given as the intensities of the fibre texture and Taylor factors are calculated both for full (FC) and relaxed (RC) constraints

Sample	*Test condition*	*Texture*			*Taylor factor*		*Elongation at fracture*
		I_{100}	I_{111}	I_{100}/I_{111}	*FC*	*RC*	
1 ($S=0$–0.3)	RT	11.5	11.5	1.0	3.10	2.80	0.33
2 ($S=0.5$–0.8)	RT	5.5	12	0.45	3.25	3.00	0.31
1 ($S=0$–0.3)	300°C	11.5	11.5	1.0	3.10	2.80	0.44
2 ($S=0.5$–0.8)	300°C	5.5	12	0.45	3.25	3.00	0.40

variations in the extruded profiles, this effect could be investigated on a single profile by comparing formability of samples taken from regions of a low and a high $\langle 100\rangle/\langle 111\rangle$ ratio, respectively. In this way variations of other parameters than texture are avoided because the samples have been subjected to identical deformation conditions.

Cylindrical tension samples of length 100 mm and diameter 6 mm were machined out from profile IE4 in the following two positions: (1) $S=0$–0.3 and (2) $S=0.5$–0.8. Tension testing was carried out at room temperature and at 300°C. For the elevated temperature the samples were held at the temperature for 5 min prior to testing in order to dissolve hardening particles. The results are given in Table III. As can be seen from the table, the best formability (taken as the elongation at fracture) was obtained for the samples of the highest $\langle 100\rangle/\langle 111\rangle$ ratio, i.e. with the lowest Taylor factor. This tendency was most strongly pronounced for tension at the elevated temperature where particle hardening is less dominating.

4. DISCUSSION

The results showed that two sharp fibre textures developed in all extrusion experiments: a $\langle 100\rangle$ and a $\langle 111\rangle$ fibre texture. Similar results are reported in the literature for axisymmetric extrusion of FCC metals, see e.g. Gertel-Kloos *et al.* (1994), Merz and Wassermann (1965), Inakazu *et al.* (1994) and Lee *et al.* (1983). Calnan (1954) reported $\langle 100\rangle$ and $\langle 111\rangle$ fibres in pure aluminium, while $\langle 111\rangle$ became more dominant in alloys. Barrett and Massalski (1966) reported a dependency on the stacking fault energy (SFE); materials with a high SFE (like Al) depict

a strong ⟨111⟩ fibre while materials with low SFE depict a strong ⟨100⟩ fibre. This is compatible with the results of Calnan (1954) since Al-alloys generally have a lower SFE than pure aluminium. This is also in agreement with the present results which show a combination of ⟨100⟩ and ⟨111⟩ for an alloy with a slightly lower SFE than pure aluminium. The results are also in agreement with Taylor simulations, see e.g. Pickus and Mathewson (1939) and Van Houtte (1984).

The present texture results showed a clearly increasing fraction of the ⟨100⟩ fibre with increasing extrusion temperature. The temperature dependency of the ⟨100⟩/⟨111⟩ ratio has been reported in the literature. Gertel-Kloos *et al.* (1994) showed that the ⟨100⟩/⟨111⟩ ratio was higher after warm extrusion than cold extrusion and Inakazu *et al.* (1994) showed an increasing amount of ⟨100⟩ fibre texture during recovery (and recrystallization). At the high temperatures of the present extrusion experiments, recovery will be of great importance, confirming the results of Inakazu *et al.* (1994). Notice that no signs of recrystallization were observed on the micrographs, see Fig. 1. Takahashi *et al.* (1973) showed that the amount of ⟨100⟩ fibre texture increased with increasing deformation temperature in an AA6063 alloy, while Dies and Wincierz (1966) found the same tendency in an Al–0.7wt%Mg–0.3wt%Fe–1.0wt%Si–0.8wt%Mn alloy. Grewen and Wassermann (1958) and Dies and Wincierz (1966) indicated that this might be due to preferred recovery in the ⟨100⟩ component, i.e. faster subgrain growth and annihilation of free dislocations. Recent results from rolling (Vatne *et al.*, 1994a,b; 1996) have demonstrated a similar preferred recovery during hot deformation of rolling for the cube orientation ({001}⟨100⟩), which is the only orientation along the ⟨100⟩ fibre which might occur after rolling. Ridha and Hutchinson (1982) explained this preferred recovery based on the unique geometry of the active slip systems in cube grains during plane strain deformation. They showed that four slip systems must be active in order to accommodate plane strain deformation. These do, however, only have two orthogonal slip Burgers vectors. This unique symmetry facilitates the annihilation of dislocations of opposite signs. A similar phenomenon might occur during axisymmetric deformation, but in that case not only the cube orientation, but the whole ⟨100⟩ fibre has this preferred recovery. No further investigations were made to confirm this mechanism or explain the increasing ⟨100⟩/⟨111⟩ ratio with increasing extrusion temperature.

However, the preferred recovery appears to be a possible and likely explanation, and this was supported by the larger subgrain size in the ⟨100⟩ fibre component.

The texture variations along the length of the profiles were rather small. This indicates homogeneous mechanical properties along the length and a rather similar flow pattern and temperature evolution during the extrusion process. The latter was also confirmed by temperature measurements on the profiles (see Table I). Note that a taper was used on the billets, i.e. the heating of the billets was regulated such that the temperature along the billet length varied in order to compensate for the friction heat that is generated during extrusion.

The through-thickness variations were larger than the variations along the profile length. The most striking result was the characteristic drop of the ⟨100⟩/⟨111⟩ ratio in the region midways between the centre and the surface of the profiles ($S = 0.25$–0.6, where S is defined as $S = 0$ in the centre and $S = 1$ at the surface). This occurred both in the front, middle and back of the profiles. The exact reason for this reduction of the ⟨100⟩ texture is not clear, but it must be due to the local flow pattern or a local temperature variation.

In the surface regions the ⟨100⟩ and ⟨111⟩ fibres were strongly rotated due to the strong shear deformation. Lee *et al.* (1983) reported a $\{110\}_{RD}\langle 335\rangle_{AD}$, i.e. grains with a ⟨110⟩ axis in the radial direction and a ⟨335⟩ axis in the axial direction. This is a component which is not much different from the Bs component ⟨011⟩{211} which develops during rolling of aluminium. The surface textures that were measured in the present work are not so different from the $\{110\}_{RD}\langle 335\rangle_{AD}$ texture component.

There were significant differences in the substructures of the two texture fibre components. The subgrains of the ⟨100⟩ texture fibre were significantly larger than in the ⟨111⟩ component. Also the average misorientation between the subgrains was larger in the ⟨100⟩ component. Both these results confirm a higher recovery rate in the ⟨100⟩ oriented grains. Concerning the stored energies in the two texture components, this was lowest in ⟨100⟩, due to the larger subgrain size. This is in agreement with the lower Taylor factor of this component and similar investigations on the cube orientation after rolling. Both the larger subgrain size and the lower amount of stored energy are important in terms of subsequent annealing. Subgrains of the ⟨100⟩ orientation will

be very potent nucleation sites for recrystallization. This explains the results by Inakazu *et al.* (1994) who found that a strong ⟨100⟩ recrystallization texture developed upon annealing. Attempts were also made to recrystallize the present alloy, but it turned out to be difficult to recrystallize, even at high annealing temperatures and long annealing times. This is no surprise when the stored energy is considered. Based on a stored energy of 6×10^4 J/m^2 the critical nucleus size for successful nucleation of a recrystallized grain actually becomes as large as 17 μm. From the subgrain size distributions (see Fig. 4) it is seen that very few subgrains are of this size. Further, it will also be difficult to reach these sizes by subgrain growth due to the large amount of recovery that has already taken place. In addition comes the fact that precipitation of small Mn-rich particles will even increase the critical nucleation size.

It is to be expected that the formability of a material will increase with increasing ⟨100⟩/⟨111⟩ ratio. This is because the orientations along the ⟨100⟩ fibre have a lower Taylor factor (i.e. softer orientations) than orientations along the ⟨111⟩ fibre (harder orientations). This has been confirmed experimentally by Takahashi *et al.* (1973) in an Al–0.6Mg–0.4Si alloy and by Dies and Wincierz (1966) in an Al–0.65Mg–0.3Fe–1.02Si–0.78Mn alloy. The measurements in the present work confirmed the dependency of the formability on texture. This could be tested for other parameters being constant by comparing tension samples taken from various positions of a single extrudate. The strain at fracture was taken as a measure for formability. The measurements clearly showed that the formability increased with increasing ⟨100⟩/⟨111⟩ ratio, in accordance with the decreasing Taylor factor. Interestingly, this effect was more pronounced at the elevated temperature than at room temperature. When testing at the elevated temperature the alloying elements will to a large extent be in solid solution, i.e. no particle strengthening will interfere and the texture becomes the determining parameter. At room temperature, on the other hand, hardening particles will contribute to the strength, so that the effect of texture on formability will be relatively smaller. Forming of extruded alloys is often undertaken at elevated temperatures where the alloying elements are in solid solution, i.e. the texture might have a significant influence on the forming operation. Thus, this result is of practical importance.

CONCLUSION

During hot extrusion of cylindrical profiles of an AA6082 alloy, ⟨100⟩ and ⟨111⟩ fibre textures develop. The ⟨111⟩ fibre is generally sharper, but the ratio ⟨100⟩/⟨111⟩ increases with increasing deformation temperature. The texture through the thickness of the profiles is rather homogeneous, but a drop in the ⟨100⟩ fibre is found in a region midways between the centre and the surface. The formability was seen to increase with increasing ⟨100⟩/⟨111⟩ ratio, particularly when testing at elevated temperatures where no particle hardening interferes. The subgrain size is larger and the misorientation between the subgrains is larger in the ⟨100⟩ texture fibre component. Thus, the recovery rate is higher in the ⟨100⟩ fibre component, and subgrains of this orientation are more potent nucleation sites for recrystallization than other subgrains. The higher recovery rate in the ⟨100⟩ texture component might explain the increase of the ⟨100⟩ texture with increasing extrusion temperature.

References

Barrett, C.S. and Massalski, T.B., *Structure of Metals*, 543, McGraw-Hill, New York (1966).

Calnan, E.A., *Acta Metall.*, **2**, 865 (1954).

Dies, K. and Wincierz, P., *Z. Metallkde.*, **57**, 227 (1966).

Gertel-Kloos, H., Brokmeier, H.-G. and Bunge, H.J., *Materials Science Forum*, **157–162**, 685, Trans. Tech. Publications (1994).

Grewen, J. and Wassermann, G., *Metall*, **12**, 523 (1958).

Inakazu, N., Kaneno, Y. and Inoue, H., *Materials Science Forum*, **157–162**, 715, Trans. Tech. Publications (1994).

Lee, D.N., Chung, Y.H. and Shin, M.C., *Scripta Metall.*, **17**, 339 (1983).

Merz, D. and Wassermann, G., *Z. Metallkde.*, **56**, 516 (1965).

Pickus, M.R. and Mathewson, C.H., *J. Inst. Metals*, **64**, 237 (1939).

Read, W.T., *Dislocations in Crystals*, McGraw-Hill, New York (1953).

Ridha, A.A. and Hutchinson, W.B., *Acta Metall.*, **30**, 1929 (1982).

Takahashi, T., Kobayashi, T. and Tokizawa, M., *J. Japan Inst. Light Metals*, **23**, 248 (1973).

Van Houtte, P., *Proc. ICOTOM 7* (Eds. C.M. Braakman *et al.*), 7, Nederland (1984).

Van Houtte, P., Software manual "MTM Taylor", Catholic University of Leuven, Belgium (1994).

Vatne, H.E., Daaland, O. and Nes, E., *Materials Science Forum*, **157–162**, 1087, Trans. Tech. Publications (1994a).

Vatne, H.E., Bolingbroke, R.K. and Nes, E., *Proc. ICAA4* (Eds. E.A. Sanders, Jr. and T. H. Starke, Jr.), 251, Atlanta (1994b).

Vatne, H.E., Shahani, R. and Nes, E., *Acta Mater.*, **44**, 4447 (1996).